Heterogeneous Catalysis

DOI: 10.1002/anie.200903581

Nanofaceted Pd–O Sites in Pd–Ce Surface Superstructures: Enhanced Activity in Catalytic Combustion of Methane**

*Sara Colussi, Arup Gayen, Matteo Farnesi Camellone, Marta Boaro, Jordi Llorca, Stefano Fabris, and Alessandro Trovarelli**

Challenges in energy and the environment call for the development of highly active catalysts, allowing for a more efficient and cleaner use of energy supplies.[1] Catalytic combustion of methane is a leading technology in emission prevention and cleanup.[2] Its main advantage over traditional flame combustion is to stabilize complete oxidation of fuel at low temperature while simultaneously controlling NO_x emissions. Catalysts yielding the highest activity at low temperatures consist of noble metals dispersed on high-surface-area oxide supports. PdO particles dispersed on oxide carriers are the most active methane combustion catalysts, but they still suffer from inadequate activity at low temperature (below 673 K) and deactivation at high temperature (above 973 K) owing to formation of metallic Pd from PdO particles.[3] This transformation is regulated by a complex dynamic of formation and decomposition of PdO to Pd under reaction conditions, which is affected by the temperature and the reaction mixture.[4] One possibility for avoiding this transformation is to disperse Pd already in the ionic form over an oxide support. Stabilization of precious metals as ionic moieties over reducible supports such as ceria (CeO_2) has been shown to be effective for several reactions, such as the water–gas shift reaction and total oxidation,[5] and the ability of ceria to stabilize Pd in a highly dispersed state is well-recognized.[6] Insertion of the precious metal into the metal oxide lattice would lead to the highest degree of dispersion for a given metal loading, with important consequences in several catalytic applications. Isolated encapsulated Pd metal in ceria as a result of a strong metal–support interaction was reported in early studies of noble-metal/ceria systems.[6,7] Solid solutions based on PdO/CeO_2 of composition $Ce_{0.99}Pd_{0.01}O_{2-\delta}$ or $Ce_{0.76}Zr_{0.19}Pd_{0.05}O_{2-\delta}$ were reported more recently and found to be active in CO/NO reaction and methane combustion;[8] this finding is also corroborated by recent density functional theory (DFT) calculations suggesting that insertion of Pd into CeO_2 surfaces provides a lower energy barrier for dissociative adsorption of methane.[9] However, stabilization of Pd-substituted ceria is difficult, and Pd segregation out of the oxide to form PdO or metallic Pd crystallites is commonly observed at high temperatures.[8]

Herein we report an ordered and stable Pd-O-Ce surface superstructure as revealed by DFT calculations on the basis of high-resolution (HR) TEM data. It results from a complex reconstruction of the (110) CeO_2 surface and leads to the opening of wide surface channels exposing highly undercoordinated oxygen atoms.

We have prepared two Pd/CeO_2 catalysts by one-step solution combustion synthesis (SCS). The new catalysts contain between 1 and 1.71 wt% Pd and are denoted SCS1 and SCS2 (Table 1). We also prepared samples of conventional Pd/CeO_2 catalysts by incipient wetness impregnation (IWI). These catalysts were prepared from two different samples of commercial ceria and had a nominal loading of 1 and 1.75 wt% Pd. They are denoted as IWI1 and IWI2 (samples a and b in Table 1).

All the materials showed excellent catalytic combustion activity. The values obtained for activation energies are similar to those reported in literature for different palladium-based catalysts.[10] Reaction rates were measured for all samples at a temperature of 553 K under differential con-

Table 1: Physicochemical properties and CH_4 combustion rates at 553 K of Pd/ceria-based catalysts.

Sample	Pd [wt%][a]	S.A. [$m^2 g^{-1}$][b]	E_a [kJ mol^{-1}]	Rate[c] [$\mu mol\, g_{Pd}^{-1}\, s^{-1}$]	Rate[c] [$10^2\, \mu mol\, m^{-2}\, s^{-1}$]
IWI1a	1.00	3.4	136	9.5	2.8
IWI1b	0.98	11.8	157	9.7	0.8
SCS1	1.09	5.4	171	25.1	5.1
IWI2a	1.72	3.3	139	5.5	2.9
IWI2b	1.74	12.2	161	7.9	1.1
SCS2	1.71	5.9	169	27.6	8.0

[a] Measured by elemental analysis. [b] BET surface area. [c] Reaction rates are reported at a constant methane conversion (less than 5%); activation energies are obtained by interpolating measured rates using the mole balance equation for plug flow reactors and taking into account the effect of water.

[*] Dr. S. Colussi, Dr. A. Gayen,[+] Dr. M. Boaro, Prof. A. Trovarelli
Dipartimento di Scienze e Tecnologie Chimiche, Università di Udine
33100 Udine (Italy)
Fax: (+39) 0432-558-803
E-mail: trovarelli@uniud.it
Dr. M. Farnesi Camellone, Dr. S. Fabris
INFM-CNR DEMOCRITOS, Theory@Elettra group
and Scuola Internazionale Superiore di Studi Avanzati (SISSA)
I-34012 Trieste (Italy)
Prof. J. Llorca
Institut de Tècniques Energètiques
Universitat Politècnica de Catalunya
08028 Barcelona (Spain)
[+] Permanent address: Department of Chemistry, Jadavpur University
Kolkata 700032 (India)

[**] This work was supported by MIUR under PRIN projects and by Regione FVG. J.L. acknowledges MEC grant ENE2006-06925. S.F. thanks "Iniziativa calcolo per la Fisica della Materia 2008" for computational resources. We thank Treibacher AG (Austria) and Grace Davison (USA) for providing samples of commercial ceria.
Supporting information for this article is available on the WWW under http://dx.doi.org/10.1002/anie.200903581.

ditions. The results show that samples prepared by SCS are always more active than conventionally prepared samples, with reaction rates per gram of noble metal that are three to five times higher. Similar conclusions are obtained if activities are measured on a surface-area basis (Table 1). The qualitative conversion profile was measured with a typical light-off curve, in which conversion is measured versus temperature in heating and cooling cycles (see Supporting Information). The light-off temperature was in the range 525–545 K for SCS samples and 555–585 K for IWI catalysts; SCS samples attained full conversion at a temperature about 100 K lower than observed in IWI samples. No deactivation was observed after ageing up to 15 h at 1173 K in all samples investigated, and identical activity profiles were also observed after repeated combustion cycles.

Ex situ XRD investigation on samples before and after catalytic reaction cycles revealed the presence of PdO crystallites in all the samples under study. No signals arising from the presence of Pd metal crystallites at low temperature were detected. In situ XRD profiles clearly show the dynamics of PdO→Pd→PdO transformation upon heating and cooling. This transformation is evident in both IWI and SCS samples; however, as determined by oxygen release and uptake measurements during temperature-programmed oxidation (TPO), in SCS samples a higher portion (ca. 6–13 wt%) of PdO initially present is not involved in the PdO→Pd transformation (details on XRD and TPO can be found in the Supporting Information). This finding points to the presence of very stable Pd–O active sites that are not involved in reversible PdO→Pd transformations. Although determination of structure–property correlations in catalysis is a very delicate issue, our findings suggest that the higher reactivity of the SCS samples is correlated with the presence of these stable Pd–O active sites.

HRTEM measurements confirmed the presence of isolated and well-dispersed PdO particles less than 5 nm in diameter in all samples investigated, both SCS and IWI. However, the SCS samples display additional features that we propose to be responsible for their higher catalytic activity. Representative lattice-fringe images of SCS2 recorded at a magnification of 10^6 are shown in Figure 1a,b together with the corresponding Fourier transform (FT) analysis (Figure 1c). White arrows in Figure 1c point to new spots that are forbidden in CeO_2, thus demonstrating the presence of an ordered supercell structure in the sample. In particular, a regular array is defined by spots at 5.7 and 8.0 Å in the FT image, which correspond to the lattice fringes clearly seen in the darker area of the HRTEM image (Figure 1a, bottom).

This supercell structure is mostly restricted to the surface or subsurface region (Figure 1b) and is clearly formed upon Pd insertion into CeO_2. It can be correlated with the portion of PdO that does not transform to Pd at high temperature and that determines the higher reactivity of the SCS samples, in agreement with recent theoretical calculations.[9] HRTEM analysis after thermal cycling confirms the presence of the surface superstructure, the features of which are not altered by exposure to high temperature. No superstructure was observed in any IWI sample, either fresh or after thermal cycling. The line scans along the $[\bar{1}10]$ and $[00\bar{1}]$ directions (Figure 2b,c) demonstrate that our SCS processing method

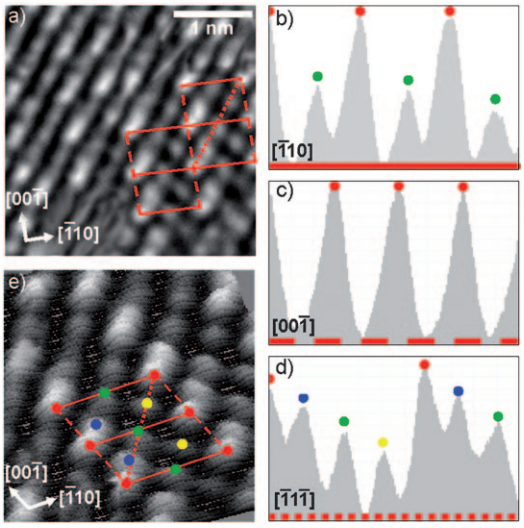

Figure 2. Profile line analysis of the periodic Pd-O-Ce superstructure. a) HRTEM image of the superstructure. b–d) Profile line analysis for sample SCS2. Profiles in (b), (c), and (d) were recorded along the $[\bar{1}10]$, $[00\bar{1}]$, and $[\bar{1}1\bar{1}]$ directions indicated in (a) by continuous, dashed, and dotted lines, respectively. All line profiles shown in (b–d) span a distance of 2.2 nm. Colored circles correspond to the atomic rows marked in the computed 3D image shown in (e); see also Figure 3a.

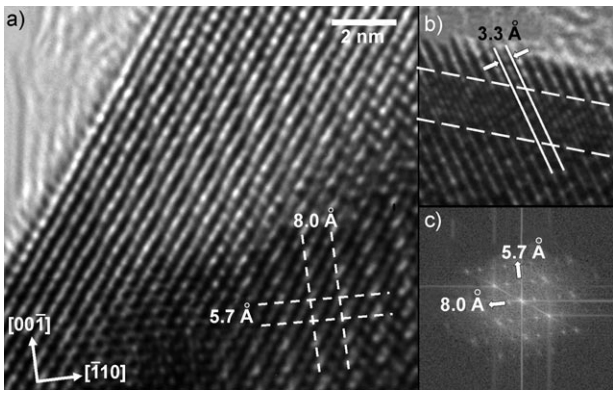

Figure 1. HRTEM images of the SCS2 sample; a) planar and b) profile view. c) Fourier transform image corresponding to the image in (a).

yields a phase with doubled unit cell along the $[\bar{1}10]$ direction. The periodicity of the ordered superstructure, 8.0 and 5.7 Å along the $[\bar{1}10]$ and $[00\bar{1}]$ directions, corresponds to a (2×1) (110) supercell containing two cation and four anion sites per layer. These considerations indicate that one out of two cation sites of the reactive Pd-O-Ce surface phase is a Pd ion.

Pd-O-Ce surface phase was further investigated with density functional theory (DFT) calculations in the pseudopotential and plane-wave framework employing the DFT + U scheme[11] (for details, see the Supporting Information). The predicted energetics and local geometries are used to rationalize the HRTEM findings. The ordered surface superstructures identified by the HRTEM analysis were modeled by (2×1) six-layer-thick supercells of the (110) surface, whose

periodicity (5.5 and 7.8 Å) closely matches the new lattice fringes at 5.7 and 8.0 Å detected by HRTEM. In these supercells in which one of the two surface Ce atoms was substituted by a Pd atom, we have considered the possible configurations and stoichiometries differing in the relative position of Ce, Pd, and O atoms as well as in the presence of O vacancies. The lowest-energy structure predicted by these calculations involves the presence of one surface oxygen vacancy that drives a strong reorganization of the (110) ceria surface. The resulting complex nanostructure is displayed in Figure 3a,c.

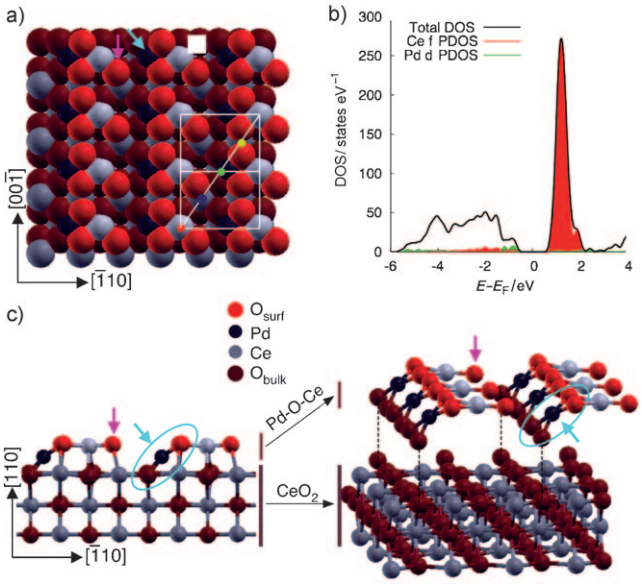

Figure 3. a) Top and c) side views of the equilibrium surface Pd-O-Ce superstructure predicted by DFT calculations. O and Ce atoms belonging to the surface superstructure phase are displayed in lighter colors. Cyan and red arrows indicate the square-planar Pd–O active site and the undercoordinated surface O atom, respectively, while a white square marks the position of the O vacancies. For clarity, the nanofaceted surface superstructure has been separated from the CeO_2 support in the side view (c). b) Density of electronic states (DOS) and projected DOS (PDOS) for the Ce 4f (red area) and Pd 4d (green area) states.

The introduction of Pd^{2+} ions into CeO_2 requires the formation of an equivalent number of O vacancies. The Pd atom substituting for a Ce atom in a C_{2v} symmetric surface site (displayed as a dark sphere and indicated by a cyan arrow) relaxes towards the second layer by 1.04 Å. This relaxation leads to a square-planar PdO_4 unit in which the Pd ion is coordinated by two O atoms of the first layer and by two O atoms of the second layer (cyan circle). The surface side views (Figure 3c) clearly show that the inward relaxation of the Pd atom towards the square-planar configuration leads to the opening of wide surface channels, similar to surface missing rows. The surface is further structured by the ordered set of O vacancies alternating with surface O atoms along the neighboring $[\bar{1}10]$ O rows and parallel to the open channels. The presence of these O vacancies results in highly undercoordinated surface O and Ce atoms, the former being two-fold coordinated, the latter having three neighboring O atoms in the surface plane (at 2.37, 2.38, and 2.24 Å) and two in the underlying layer (at 2.48 Å). All Ce cations have the formal 4+ oxidation state, and no reduction to Ce^{3+} arises from the O vacancies. This situation is evident in the calculated density of electron states (Figure 3b), where the band gap is between the occupied Pd 4d and Ce 4f states, while the filled Ce 4f gap states characteristic of reduced ceria[11,12] are absent.

The general tendency of d^8 Pd^{2+} to form square-planar complexes in solution[13] underpins the stability of the active Pd-O-Ce surface superstructure. We also note that this square-planar geometry closely resembles the one in bulk PdO,[14] where the calculated Pd–O bond lengths (2.05 Å) and O-Pd-O angles (84.0 and 96.0°) are quite comparable to the ones in the surface Pd-O-Ce superstructure (2.04 Å, 86.5 and 92.5°). Stabilization of Pd^{2+} in a four-coordinate pseudo-square-planar geometry similar to that in PdO has also been observed in mesoporous Pd/Al_2O_3 catalyst for oxidation of allylic alcohols.[15] The ordered surface superstructure resulting from our one-step combustion synthesis can be seen as composed of CeO_2 (110) and PdO (111) nanofacets separated by open channels along $[\bar{1}10]$ resulting from the inward relaxation of the Pd atoms. This structure, formed by an ordered assembly of substituted Pd ions and surface oxygen vacancies, exposes highly undercoordinated O atoms (red arrow) in front of the PdO nanofacets that are likely to play an important role in the activation of methane.

The Pd-O-Ce surface nanostructure identified by the DFT simulations is corroborated by the HRTEM data. According to the proposed surface model (Figure 3a), a linescan along the $[\bar{1}1\bar{1}]$ direction should sample four cation sites, yielding different scattering intensities arising from the different local environments. Indeed, the HRTEM linescan along $[\bar{1}1\bar{1}]$ (Figure 2d,e) displays four peaks, the origin of which can be rationalized by the presence of a substituted Pd atom and a surface O vacancy. The highest intensity (red circle in Figure 2e) arises from a Ce column terminating with a surface Ce atom (red circle in Figure 3a). The other column of Ce atoms that reaches the supercell surface (green circle in Figure 2e) is terminated by a Pd atom (green circle in Figure 3a), which, being lighter than Ce, reduces the measured intensity of the signal from that column. The lowest intensity (yellow circle in Figure 2e) is instead due to a Ce column that terminates below the surface (yellow circle in Figure 3a) and is therefore screened by the charge density of two O atoms. Finally, the Ce column terminating below the surface (blue circle in Figure 2e and Figure 3a) is instead only partially screened owing to the presence of the O vacancy, and therefore it has a scattering intensity which is higher than the former fully screened Ce column (yellow circle in Figure 2e) but lower than a Ce column terminating at the surface (red circle in Figure 2e).

The Pd-O-Ce surface superstructure is consistent with the asymmetry in the linescan along the $[\bar{1}10]$ direction. The peak marked by the green circle in Figure 2b is not equidistant from the highest peaks (red circles) but is off-center by approximately 0.2–0.3 Å. This asymmetry is expected from the shift of the Pd atom towards the square-planar coordination and away from the neighboring surface O vacancy. The

Pd atom therefore adds scattering intensity weight that is off-center with respect to the underlying Ce column, thus leading to the observed asymmetry in the linescan.

Our study shows that both structural and chemical features of ordered Pd-O-Ce moieties contribute to the higher activity observed in the oxidation of methane. These features are related to 1) the close structural similarity between the Pd–O moiety in this Pd-O-Ce phase and that in PdO surfaces, and to 2) the presence of the ordered undercoordinated surface O atoms in front of the Pd–O moiety that are likely to be more labile. The new phase we have identified provides an example of ultra-highly dispersed and stable PdO within an oxide carrier with significant electronic and geometric effects. Concerning the reaction pathway for methane activation, we can foresee that many of the parameters identified previously[9,16] could play an important role also in the new phase identified herein, but the PdO_4 square-planar superstructure may open new surface-specific activation channels. The possibility of stabilizing these highly dispersed metal centers in ceria by formation of stable, regular surface superstructure opens new and exciting perspectives in attaining highly efficient and durable catalysts, with potential implications in a wide range of catalytic reactions.

Experimental Section

Pd/CeO_2 catalysts containing between approximately 1 and 1.71 wt% Pd were prepared by one-step solution combustion synthesis (SCS) using $(NH_4)_2Ce(NO_3)_6$ (Treibacher A.G., Austria) and $Pd(NO_3)_2$ (Johnson Matthey Chemicals, England) as oxidizers and oxalyldihydrazide ($C_2H_6N_4O_2$, ODH) as reducer (for further details, see the Supporting Information). The solution was transferred into a pre-heated muffle furnace maintained at approximately 623 K, in which the combustion reaction took place. Conventional catalysts were prepared by the incipient wetness technique starting from a solution of 10 wt% $Pd(NO_3)_2$ (Aldrich, 99.999%). The solution was added dropwise to CeO_2 supports previously calcined at 1173 K for 4 h. After impregnation, the samples were dried at 393 K for 16 h and then calcined at 1173 K for 4 h.

Catalytic tests were carried out in a quartz tubular reactor (i.d. 6 mm) with 0.5 vol% CH_4, 2 vol% O_2 in helium with a gas hourly space velocity (GHSV) of approximately 200000 h^{-1}. Effluent gases were monitored with an ABB Advance Optima IR gas analyzer.

Received: July 1, 2009
Revised: August 28, 2009
Published online: October 2, 2009

Keywords: ceria · density functional calculations · heterogeneous catalysis · nanostructures · palladium

[1] N. Armaroli, V. Balzani, *Angew. Chem.* **2007**, *119*, 52 – 67; *Angew. Chem. Int. Ed.* **2007**, *46*, 52 – 66.
[2] R. E. Hayes, S. T. Kolaczkowski, *Introduction to Catalytic Combustion*, Gordon and Breach Science Publishers, Amsterdam, **1997**.
[3] a) D. Ciuparu, M. R. Lyubovsky, E. Altman, L. Pfefferle, A. Datye, *Catal. Rev. Sci. Eng.* **2002**, *44*, 593 – 649; b) P. Gélin, M. Primet, *Appl. Catal. B* **2002**, *39*, 1 – 37.
[4] a) R. J. Farrauto, M. C. Hobson, T. Kennelly, E. M. Waterman, *Appl. Catal. A* **1992**, *81*, 227 – 237; b) J. G. McCarty, *Catal. Today* **1995**, *26*, 283 – 293; c) G. Zhu, J. Han, D. Yu, Y. Zemlyanov, F. H. Ribeiro, *J. Phys. Chem. B* **2005**, *109*, 2331 – 2337; d) J. D. Grunwaldt, N. van Vegten, A. Baiker, *Chem. Commun.* **2007**, 4635 – 4637.
[5] a) Q. Fu, H. Saltsburg, M. Flytzani-Stephanopoulos, *Science* **2003**, *301*, 935 – 938; b) G. Groppi, C. Cristiani, L. Lietti, C. Ramella, M. Valentini, P. Forzatti, *Catal. Today* **1999**, *50*, 399 – 412; c) L. Murrell, R. T. Carlin, *J. Catal.* **1996**, *159*, 479 – 490.
[6] a) A. Trovarelli, *Catal. Rev. Sci. Eng.* **1996**, *38*, 439 – 520; b) S. Bernal, J. J. Calvino, J. M. Gatica, C. Lopez Cartez, J. M. Pintado in *Catalysis by Ceria and Related Materials* (Ed.: A. Trovarelli), Imperial College, London, **2002**, pp. 85 – 168.
[7] a) C. Binet, A. Jadi, J. C. Lavalley, M. Boutonnet-Kizling, *J. Chem. Soc. Faraday Trans.* **1992**, *88*, 2079 – 2084; b) A. Badri, C. Binet, J. C. Lavalley, *J. Chem. Soc. Faraday Trans.* **1996**, *92*, 1603 – 1608.
[8] a) P. Bera, K. C. Patil, V. Jayaram, G. N. Subbanna, M. S. Hegde, *J. Catal.* **2000**, *196*, 293 – 301; b) K. R. Priolkar, P. Bera, P. R. Sarode, M. S. Hegde, S. Emura, R. Kumashiro, N. P. Lalla, *Chem. Mater.* **2002**, *14*, 2120 – 2128; c) A. Primavera, A. Trovarelli, C. de Leitenburg, G. Dolcetti, J. Llorca, *Stud. Surf. Sci. Catal.* **1998**, *119*, 87 – 92.
[9] A. D. Mayernick, M. J. Janik, *J. Phys. Chem. C* **2008**, *112*, 14955 – 14964.
[10] G. Zhu, J. Han, D. Y. Zemlyanov, F. H. Ribeiro, *J. Am. Chem. Soc.* **2004**, *126*, 9896 – 9897.
[11] S. Fabris, G. Vicario, G. Balducci, S. de Gironcoli, S. Baroni, *J. Phys. Chem. B* **2005**, *109*, 22860 – 22867.
[12] a) S. S. Nolan, M. Nolan, S. P. Parker, G. W. Watson, *Surf. Sci.* **2005**, *595*, 223 – 232; b) P. R. B. Loschen, C. Loschen, J. Carrasco, K. M. Neyman, F. Illas, *Phys. Rev. B* **2006**, *75*, 035115; c) J. L. F. Da Silva, M. V. Ganduglia-Pirovano, J. Sauer, V. Bayer, G. Kresse, *Phys. Rev. B* **2006**, *75*, 045121; d) S. Fabris, S. de Gironcoli, S. Baroni, G. Vicario, G. Balducci, *Phys. Rev. B* **2005**, *71*, 041102.
[13] F. A. Cotton, G. Wilkinson, C. A. Murillo, M. Bochmann, *Advanced Inorganic Chemistry*, 6th ed., Wiley, New York, **1999**, p. 977.
[14] J. Waser, H. A. Levy, S. A. Peterson, *Acta Crystallog.* **1953**, *6*, 661 – 663.
[15] S. F. J. Hackett, R. M. Brydson, M. H. Gass, I. Harvey, A. D. Newmann, K. Wilson, A. F. Lee, *Angew. Chem.* **2007**, *119*, 8747 – 8750; *Angew. Chem. Int. Ed.* **2007**, *46*, 8593 – 8596.
[16] D. Knapp, T. Ziegler, *J. Phys. Chem. C* **2008**, *112*, 17311 – 17318.

